Biosensors and Bioelectronics 131 (2019) 185–192

Contents lists available at ScienceDirect

Biosensors and Bioelectronics

journal homepage: www.elsevier.com/locate/bios

Single-particle characterization of theranostic liposomes with stimulus sensing and controlled drug release properties

Chaoxiang Chen[a,*], Kaimin Gao[b], Hong Lian[b], Chen Chen[b], Xiaomei Yan[b,*]

[a] Department of Biological Engineering, College of Food and Biological Engineering, Jimei University, Xiamen, Fujian 361021, People's Republic of China
[b] MOE Key Laboratory of Spectrochemical Analysis & Instrumentation, Key Laboratory for Chemical Biology of Fujian Province, Collaborative Innovation Center of Chemistry for Energy Materials, Department of Chemical Biology, College of Chemistry and Chemical Engineering, Xiamen University, Xiamen, Fujian 361005, People's Republic of China

ARTICLE INFO

Keywords:
Single-particle analysis
Flow cytometry
Multiparameter characterization
Stimuli-responsive liposomes
Nanosensor

ABSTRACT

Stimuli-responsive nanotheranostic systems, integrated with diagnosis and treatment features, have recently emerged and attracted much interest. However, most of the research mainly focuses on the novelty of nanomaterials, and undervalues the significance of single-particle characterization which can provide detailed physical and biochemical information for performance evaluation and heterogeneity assessment. Due to the small particle size and low content of functional modules, high throughput and multiparameter analysis of individual stimuli-responsive nanoparticles still remains challenging. Here, fabricating a reactive oxygen species (ROS)-responsive liposome (Lipo@BODIPY11) and taking it as an example, we report the development of a strategy for theranostic nanoparticle characterization by a laboratory-built nano-flow cytometer (nFCM). Coincident detection of light scatter and fluorescence intensity provided a measure for liposome quality assessment. Theranostic performance referred to stimuli-responsive capability and drug release behavior upon ROS treatment were obtained in minutes. Besides, the dissociation of functional modules from liposomes and the formation of aggregates under high modification degree were revealed, which was otherwise masked by ensemble-averaged methods. At last, consistent results were also observed in intracellular studies. This nFCM-based method provides a comprehensive approach for the proof-of-principle study, heterogeneity assessment and quality control of biochemical nanosensors and theranostic nanomaterials.

1. Introduction

Nanotheranostics, which integrates diagnostic and therapeutic functions in a single nanomaterial, has emerged as a promising platform for cancer treatment (H. Chen et al., 2017; Muthu et al., 2014b). Nanotheranostics enables tumor markers detection, pathological tissues visualization and cancer cell killing simultaneously, which would significantly improve the anticancer efficacy (Jo et al., 2016; Muthu et al., 2014a). Advanced properties such as controlled drug release can be accessed by introducing stimuli-responsive modules to the nanocarriers (Li et al., 2014; Wang et al., 2017). Benefited from the advantages of co-encapsulation of diagnostic, therapeutic and functional molecules in a single particle, real-time diagnosis and treatment in response to endogenous or exogenous stimulus can be achieved (Bolla et al., 2018; Li et al., 2018; Qian et al., 2017; Yang et al., 2018).

Among the cancer-related variations, elevated ROS production has been proved to be in close association with cancer progression and considered as an important pathological marker and therapeutic target (Liu et al., 2018; Schumacker, 2015). This abnormal alteration has inspired the development of various ROS-responsive drug delivery systems (Kim et al., 2015; Saravanakumar et al., 2017). Among them, nanotheranostics affording both diagnostic and therapeutic functions in a single particle have shown unprecedented potential in cancer treatment (Q. Chen et al., 2017; Li et al., 2016; Zhang et al., 2018).

Generally, stimuli-responsive theranostic depends on the modification of functional molecules to the nanoparticles (Chen et al., 2015; Karimi et al., 2016; Mura et al., 2013). Controlled distribution of these functional molecules in individual nanoparticle is essential for the successful theranostic application. Therefore, it is important to ensure the proper functionalization of nanocarriers, such as through investigating the existence (or not) of some particles with over-/insufficient functionalization degree and other undesired materials which would hamper the overall theranostic performance. Therefore, multiparameter characterization at the single-particle level is implemented

* Corresponding authors.
E-mail addresses: cxchen@jmu.edu.cn (C. Chen), xmyan@xmu.edu.cn (X. Yan).

https://doi.org/10.1016/j.bios.2019.02.016
Received 3 January 2019; Received in revised form 4 February 2019; Accepted 10 February 2019
Available online 19 February 2019
0956-5663/

to reveal particle heterogeneity and obtain distribution of properties on stimulus sensing capability and controlled drug release efficiency (Bayford et al., 2017; Muhlebach et al., 2015). However, the lack of state-of-the-art techniques has become one of the major challenges in this field, which will seriously impede the development of stimuli-responsive nanotheranostics (Cho et al., 2013; Mourdikoudis et al., 2018; Rosenblum et al., 2018).

Integrating light scattering with strategies for single molecule fluorescence detection in a sheathed flow, a nano-flow cytometer (nFCM) has been developed to achieve single lipid-nanoparticle detection with size down to 40 nm, such as liposome and exosomes (C.X. Chen et al., 2017; Tian et al., 2018; Zhu et al., 2014). Taking advantages of the multiparameter quantification ability of nFCM, here we report a strategy for the characterization of a stimuli-responsive nanotheranostics with ROS sensing and controlled drug release features. Firstly, by insertion of a lipid oxidation sensor, C11-BODIPY (581/591), to the bilayer of liposomes, we synthesized a ratiometric fluorescent nanoprobe for ROS detection. Using nFCM, changes in the distribution of ROS-induced fluorescence intensity, along with physical properties such as particle size and concentration could be measured in minutes. We also revealed the ROS-triggered detachment of the functional molecules and the formation of aggregation for liposomes with high functionalization degree, which was often masked and ignored by traditional ensemble-averaged methods. Then a chemotherapy drug, Mitoxantrone (MXT), was encapsulated into C11-BODIPY (581/591) functionalized liposomes, and the ROS sensing and drug release behaviors were simultaneously characterized by nFCM. Furthermore, the intracellular theranostic effect was investigated to prove the applicability of the as-fabricated nanomaterials.

2. Experimental section

2.1. Reagents and chemicals

Phospholipids and cholesterol (CHOL) were purchased from Avanti Polar Lipids, Inc. (Alabaster, AL). C11-BODIPY (581/591) was purchased from Invitrogen (Carlsbad, CA). Mitoxantrone dihydrochloride was purchased from Sigma (St. Louis, MO). PD-10 desalting columns and polycarbonate membrane filters were purchased from GE Healthcare Life Sciences (Piscataway, NJ). All other reagents were purchased from Beijing Chemical Reagent Company (Beijing, China).

2.2. Preparation of C11-BODIPY (581/591) modified liposomes

C11-BODIPY (581/591) modified liposomes were prepared by thin-film hydration followed by extrusion (C.X. Chen et al., 2017). Unless otherwise noted, the Lipo@BODIPY11 formulation was stated as follows. 1,2-dioleoyl-sn-glycero-3-phosphocholine (DOPC), cholesterol, 1,2-distearoyl-sn-glycero-3-phosphoethanolamine-N-[methoxy(polyethylene glycol)-2000] (DSPE-PEG2000) and C11-BODIPY (581/591) were dissolved and mixed in chloroform at a molar ratio of 57:38:5:5 with a total lipid content of 20 μmol. Then the lipid mixture was dried on a rotary evaporator to form a thin film and kept in vacuo for 6 h to remove the residual solvent. The lipid film was hydrated in 1 mL PBS solution at R.T. for 1 h and followed by sequential extrusion through PC membrane filters with pore sizes of 400, 200 nm and 50 nm for 20 cycles, respectively.

For the preparation of MXT loaded liposomes, the dried lipid film was hydrated in 250 mM ammonium sulfate, and the liposome suspension was dialyzed against PBS to establish a transmembrane ammonium gradient for drug loading. MXT was added to liposomes with a drug-to-lipid molar ratio of 1:10 and purified through Sephadex G-25 column to remove unloaded MXT.

2.3. Fluorescence spectroscopy analysis

The Lipo@BODIPY11 samples were subjected to H_2O_2 with concentration ranged from 0.01 mM to 10 mM and analyzed by a spectrofluorometer. The fluorescence spectrum was measured, and signal intensity at 515 nm and 595 nm was recorded to quantitatively investigate the H_2O_2-triggered fluorescence change.

2.4. Multiparameter analysis by nFCM

A previously built nFCM system was used for the characterization of Lipo@BODIPY11 with minor modification (C.X. Chen et al., 2017). The detail of nFCM was described in Supplemental information. Lipo@BODIPY11 with/without H_2O_2 treatment was loaded to nFCM system with a concentration at ~10^9 particles/mL. Events with signals concurrently measured on all three channels, SS, green FL and orange FL, were referred to well-prepared particles with C11-BODIPY (581/591) modification, which were used for data analysis. For drug loaded liposomes, a second laser of 642 nm was settled to excite the intrinsic fluorescence of MXT.

2.5. ROS-activated intracellular ratiometric fluorescence response

For the intracellular detection of ROS-activated ratiometric fluorescence response, 0.5 mol% DSPE-PEG2000-FA was added to prepare folate-conjugated liposomes, Lipo-FA@BODIPY11. Then KB cells were incubated with Lipo-FA@BODIPY11 at a final lipid concentration of 100 μM for 1 h, 3 h, 6 h, 12 h and 24 h. For the study of the influence of exogenous ROS, 500 μM H_2O_2 or a mixture of 500 μM H_2O_2 and 2 mM NAC was added to specific wells three hours before the liposome treatment. Afterward, the cells were analyzed immediately by a BD FACSAria III flow cytometer. The filters used for the ratiometric fluorescence analysis were 530/30 nm and 610/20 nm under 488 nm excitation.

2.6. Simultaneous intracellular ROS sensing and drug release analysis

MXT loaded folate liposomes with or without C11-BODIPY (581/591) modification were incubated with KB cells for 1 h, 3 h, 6 h, 12 h and 24 h, respectively. Then the samples were excited with 488 nm and 633 nm lasers for the fluorescence detection of C11-BODIPY and MXT by the flow cytometer. The filters used for fluorescence detection of C11-BODIPY and MXT were 530/30 nm, 610/20 nm and 660/20 nm.

2.7. CCK-8 cytotoxicity analysis

CCK-8 assay was applied to assess the liposome cytotoxicity. KB cells were seeded in 96-well plates and cultured in RPMI-1640 medium for 6 h. Then liposomes or free MXT with drug concentration ranging from 0.1 to 10 μM (or 1–100 μM of total lipid concentration) were added to KB cells and cultured for another 12 h. To analyze the impact of exogenous ROS, cells were treated with 200 μM H_2O_2 and incubated for additional 12 h. Afterward, 10 μL CCK-8 solution was added to each well for 2 h according to the instructions. The absorbance at 450 nm was measured on a Spectra MAX 190 microplate reader. Measurements were carried out in triplicate.

3. Results and discussion

3.1. H_2O_2-induced ratiometric fluorescence response of a ROS-responsive liposomes, Lipo@BODIPY11

C11-BODIPY (581/591) is an established ratiometric fluorescent sensor for ROS detection in cells and membranes (Drummen et al., 2004, 2002). Owing to the amphipathic characteristic, it can be easily inserted into liposomes and become a nanoprobe for ROS detection.

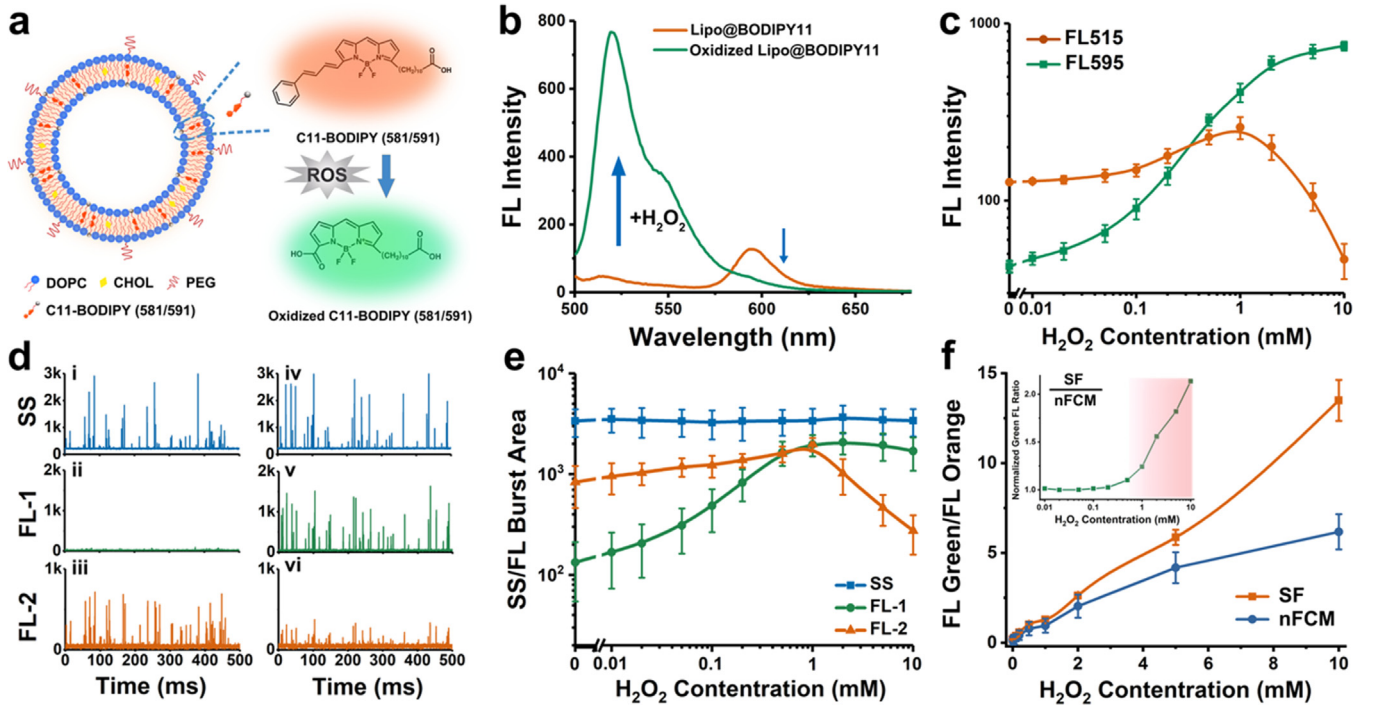

Fig. 1. Fluorescent analysis of C11-BODIPY (581/591) modified liposomes, Lipo@BODIPY11, by spectrofluorometer and nFCM. a) Schematic of C11-BODIPY (581/591) oxidation in liposomes by ROS, leading to the fluorescence change. b) Fluorescence spectra of Lipo@BODIPY11 upon 5 mM H_2O_2 treatment by spectrofluorometer. c) H_2O_2 concentration-dependent changes in FL515 and FL595 of Lipo@BODIPY11. d) Representative SS, FL-1 and FL-2 burst traces of Lipo@BODIPY11 without (i-iii) or with (iv-vi) H_2O_2 treatment. e) H_2O_2 concentration-dependent changes in SS, FL-1 and FL-2 burst area of Lipo@BODIPY11. f) Comparison of the H_2O_2-triggered ratiometric fluorescence changes of Lipo@BODIPY11 by spectrofluorometer and nFCM. The error bars represent the standard deviation from three independent measurements in SF-based plots, and the interquartile range of the distribution in nFCM results.

Therefore, a C11-BODIPY (581/591) modified liposome, Lipo@BODIPY11, was prepared by thin-film hydration method followed by extrusion (Zhang, 2017).

The ROS sensing capability of Lipo@BODIPY11 was investigated via the H_2O_2-induced ratiometric fluorescence change by a spectrofluorometer (SF). In the absence of H_2O_2, Lipo@BODIPY11 showed a strong signal at 595 nm and emitted dim fluorescence at 515 nm. Upon the addition of 5 mM H_2O_2, a significant increase of FL515 along with a fluorescence decline at 595 nm was observed, due to the ROS-induced oxidation of the diene between the BODIPY chromophore and the phenyl group (Fig. 1b). The oxidized C11-BODIPY (581/591) without extension over the phenyl moiety retroceded to the initial green fluorescence of the BODIPY chromophore (Drummen et al., 2004). With the increase of H_2O_2, the FL595 intensity boosted slightly at first and then significantly dropped off compared to the continuously growing FL515 intensity (Fig. 1c). A plausible explanation for the FL595 increase under low levels of H_2O_2 stimulation is the oxidation induced fluorescence dequenching of C11-BODIPY (581/591) on liposome bilayers.

3.2. nFCM characterization of Lipo@BODIPY11

To confirm the homogenous insertion of C11-BODIPY (581/591) and analyze the ROS-induced variation on fluorescence intensity and other physicochemical properties, such as size distribution and particle concentration, a nFCM-based methodology was developed for the single-particle characterization of Lipo@BODIPY11. As individual liposomes passing sequentially through the tightly focused laser beam of nFCM, side scatter (SS) and fluorescence (FL) signals were simultaneously detected. Fig. 1d showed the representative SS and FL burst traces of Lipo@BODIPY11 with/without H_2O_2 treatment. The concomitantly detected peaks and the positive correlation in signal intensity on both channels, SS and Orange FL (FL-2), proved the successful C11-BODIPY (581/591) modification (Fig. 1d, i&iii). After subjected to 5 mM H_2O_2, the intensity of green FL (FL-1) remarkably increased along with the decline of orange FL, which was in consistency with the spectrofluorometer-based results (Fig. 1d, iv-vi). The constant SS intensity and the consistent one-to-one correspondence on three channels showed that there was no detectable compromise in particle integrity upon H_2O_2 treatment. Compared with the results obtained on the spectrofluorometer, a significant discrepancy of green FL intensity and the ratio of green FL to orange FL was observed, especially when H_2O_2 concentration was above 1 mM (Fig. 1e&f). According to the previous research of the H_2O_2 induced structure change of C11-BODIPY (581/591), we attributed this phenomenon to the hydrophobicity change. In detailed, the diene conjugated phenyl moiety attached to the BODIPY core is hydrophobic, accounted for its tightly insertion in liposome bilayers. Under exposure to oxidant, this group is converted to the hydrophilic carboxyl group, which reduces the overall hydrophobicity of the whole molecule. With the continuous formation of hydrophilic groups, some oxidized C11-BODIPY (581/591) will detach from liposomes and diffuse to the solution. Using bulk analysis methods like spectrofluorometer, the detected FL intensity were attributed to the whole solution, including the liposomes and the detached fluorophores. For nFCM, only particles with scattering signals would be counted as an individual event and the corresponding SS & FL signals were recorded for data processing. Therefore, the detached fluorophores made no contribution to the signal intensity, which caused the discrepancy of green FL intensity measured by nFCM and spectrofluorometer. As the increase of ROS, more C11-BODIPY (581/591) molecules were oxidized and detached from liposomes, which made the discrepancy more significant. Apart from the ratiometric fluorescence detection, nFCM was also applied to obtain the particle concentration and size distribution profile of Lipo@BODIPY11 (Fig. S4&S5).

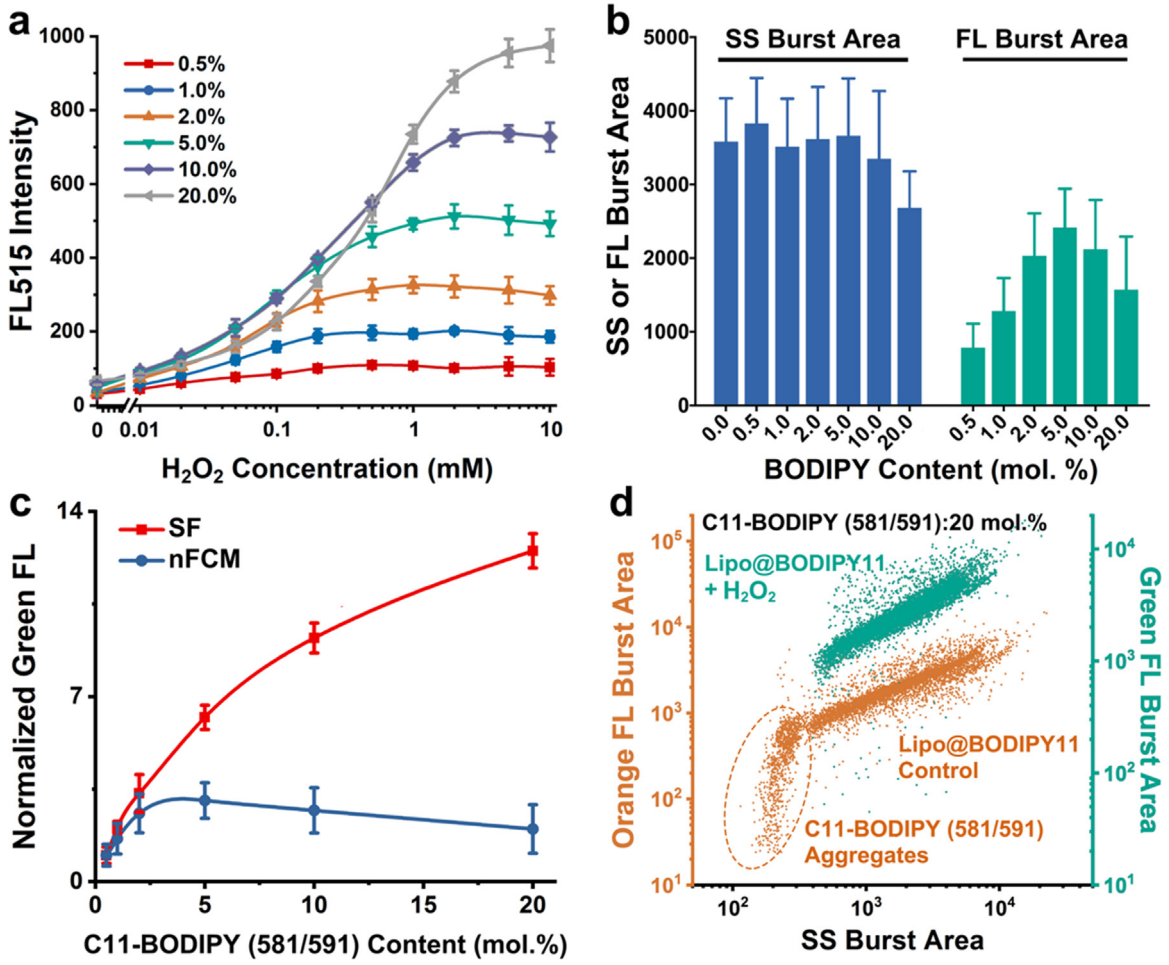

Fig. 2. Investigation of C11-BODIPY (581/591) content on the ROS sensing performance of Lipo@BODIPY11. a) Spectrofluorometer analysis of the H_2O_2 concentration-dependent changes in FL515 of Lipo@BODIPY11 with various C11-BODIPY (581/591) content. b) nFCM analysis of the H_2O_2 triggered SS and FL-1 change of Lipo@BODIPY11 with various C11-BODIPY (581/591) content. c) Comparison of the normalized green fluorescence measured by spectrofluorometer and nFCM. d) Bivariate dot-plots of SS versus orange/green fluorescence for Lipo@BODIPY11 with 20% C11-BODIPY (581/591) with or without H_2O_2 treatment, respectively. The error bars represent the standard deviation from three independent measurements in SF-based plots, or the interquartile range of the distribution in nFCM results. (For interpretation of the references to color in this figure, the reader is referred to the web version of this article.)

3.3. nFCM guided optimization of C11-BODIPY (581/591) content

Firstly, liposomes with various molar content (%) of C11-BODIPY (581/591) were fabricated. Then FL515 intensity was recorded and plotted verse H_2O_2 concentration to analyze the ROS induced fluorescence change by a spectrofluorometer (Fig. 2a). As expected, FL515 intensity boosted initially and then leveled out with the increase of H_2O_2 concentration. Liposomes with most C11-BODIPY (581/591) molecules would reach a highest plateau, but displayed a compromised sensitivity to H_2O_2 stimulation in the lower concentration range. As for the nFCM analysis, we found C11-BODIPY (581/591) content lower than 10% had negligible influence on SS intensity, which proved no integrity compromise of liposomes upon H_2O_2 treatment (Fig. 2b). Green FL intensity increased firstly along with the increment of C11-BODIPY (581/591) concentration but then suddenly dropped off when the molar content of C11-BODIPY (581/591) was above 10%. Fig. 2c demonstrated a growing discrepancy of green FL intensity (normalized by the green FL intensity of liposomes containing 0.5% C11-BODIPY (581/591)) measured by nFCM and spectrofluorometer. This further consolidated the speculation that H_2O_2-triggered hydrophobicity change of C11-BODIPY (581/591) would lead to its detachment from the nanocarriers, especially for liposomes with higher C11-BODIPY (581/591) content. In addition, bivariate dot-plots of SS and FL of Lipo@BODIPY11 with 20% C11-BODIPY (581/591) were illustrated in Fig. 2d. In the absence of H_2O_2, unmodified C11-BODIPY (581/591) would self-assemble to form small aggregates with weaker SS and orange FL signals compared to Lipo@BODIPY11 (Fig. 2d, orange dots). Owing to the increased hydrophilicity of C11-BODIPY (581/591) upon H_2O_2 oxidization, the aggregates were disassembled to individual molecules, which could no longer be detected by nFCM (Fig. 2d, green dots). Collectively, we found that liposomes with higher functionalization degree showed a stronger tendency to undergo ROS-induced detachment of C11-BODIPY (581/591). But over-modification (> 10%) lead to the formation of undesired C11-BODIPY (581/591) aggregates, which might influence the ROS-responsive behavior of Lipo@BODIPY11.

3.4. Multiparameter characterization of drug loaded Lipo@BODIPY11

We adopted this nFCM-based method to investigate ROS-triggered drug release profile along with the ratiometric fluorescence change of drug encapsulated Lipo@BODIPY11. Firstly, loading an anti-cancer chemotherapeutic drug mitoxantrone (MXT) to liposomes with 5% C11-BODIPY (581/591), a nanoplatform (Lipo@BODIPY11&MXT) with theranostic features was prepared (Fig. 3a). Using remote loading approach, anthracyclines such as MXT could be efficiently transferred from bulk solution to the inner core of liposomes. Meanwhile, the intrinsic fluorescence of MXT was significantly quenched due to the

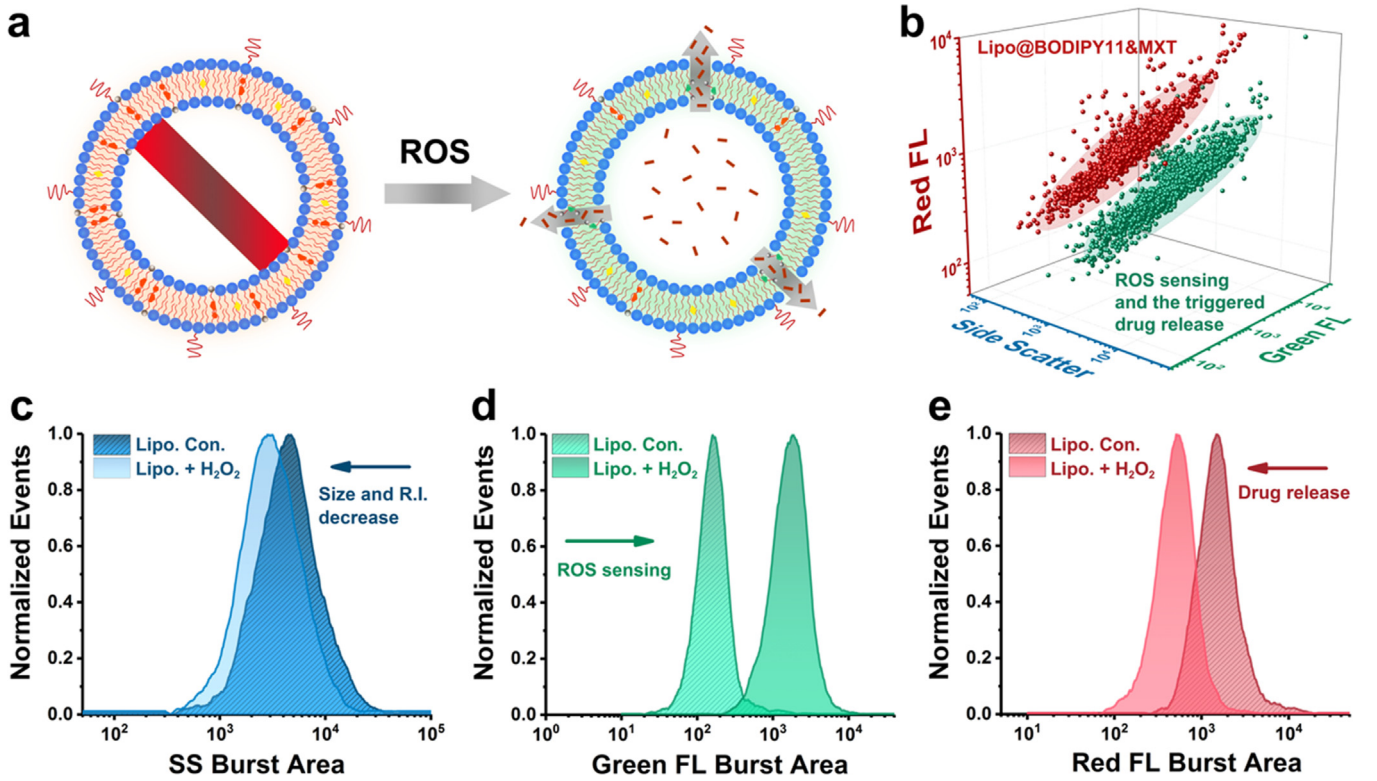

Fig. 3. Simultaneous detection of the ROS sensing and controlled drug release behavior of Lipo@BODIPY11&MXT by nFCM. a) Schematic illustration of the simultaneous fluorescence change and drug release behavior of Lipo@BODIPY11&MXT triggered by ROS. b) Three-dimensional dot-plots of SS, green FL and red FL for Lipo@BODIPY11&MXT with/without H_2O_2 treatment. c-e) The H_2O_2 triggered SS, green FL and red FL change.

highly-concentrated aggregation inside liposomes. Thanks to the superior sensitivity of nFCM, the fluorescence of MXT could still be detected despite of the dramatic quenching effect. Therefore, three-parameter correlation analysis was conducted to evaluate the co-existence of C11-BODIPY (581/591) and MXT on a single liposome, which was essential to ensure the theranostic properties. According to the results illustrated in Fig. 3b, nearly 100% insertion of C11-BODIPY (581/591) and encapsulation of MXT were achieved. After treated with 5 mM H_2O_2, the concurrent signal change of SS, green FL and red FL confirmed the ROS-responsive theranostic property of Lipo@BODIPY11 &MXT at single-nanoparticle level. The decrease of SS intensity was a result of drug-release caused deformation and refractive index change of liposomes (Fig. 3c). The shifts of green FL and red FL were referred to the ROS sensing and the corresponding drug release behavior, respectively (Fig. 3d&e).

Lipo@BODIPY11&MXT with different C11-BODIPY (581/591) content were fabricated and the ROS-triggered variations in SS, green FL and red FL intensity were simultaneously detected. The green FL intensity varied identically as the liposomes without MXT. The red FL intensity remained unchanged and then suddenly dropped off when C11-BODIPY (581/591) content exceeds 2%, indicating the leakage of MXT from liposomes (Fig. 4a). The similar SS variation pattern as red FL further proved the effective drug release process. Although a more significant releasing process was observed for liposomes with higher C11-BODIPY (581/591) content, the compromised ROS sensing sensitivity and the aggregate formation would largely limit their application. Therefore, MXT loaded liposomes with 5% C11-BODIPY (581/591) showed an optimal theranostic effect and were chosen for the following research. The simultaneous signal changes on three channels were recorded to investigate the ROS sensing and controlled drug release profiles under various H_2O_2 concentration or incubation time (Fig. 4b& c). The bivariate plots between green to orange FL ratio (FL_{green}/FL_{orange}) and the red FL intensity (FL_{red}) derived from Fig. 4b offered a more straightforward insight into their relationship (Fig. 4d). Moreover, we also analyzed the incubation time dependent signal changes on SS, green FL and red FL of Lipo@BODIPY11&MXT without H_2O_2 treatment or liposomes without C11-BODIPY (581/591) modification (Fig. S6). It showed no obvious variation on all three channels during 24 h incubation period, which further proved that the theranostic function was attributed to the insertion of C11-BODIPY (581/591).

3.5. ROS-triggered intracellular fluorescence change and drug release

To investigate the ratiometric fluorescence change induced by endogenous ROS, a Lipo@BODIPY11 with folate modification (Lipo-FA@ BODIPY11) was fabricated and internalized by KB cells through folate receptor mediated endocytosis (Patil et al., 2016; Zwicke et al., 2012). Analyzed by a conventional flow cytometer (FCM), the time-dependent elevation of fluorescence intensity on both channels (FL_{530} and FL_{610}) was observed, which could be attributed to the increased internalization level or the ROS triggered colorimetric response (Fig. 5a&b). To clarify that, the ratio between both channel (FL_{530}/FL_{610}) was calculated and plotted verse the incubation time (Fig. 5c). A proportional relationship between the increased F_{530}/F_{610} value and the prolonged incubation time was observed in Fig. 5c, which substantially proved the existence of a ROS activated fluorescence response.

To further elucidate the role of ROS concentration in the induction of ratiometric fluorescence change, KB cells were treated with H_2O_2 or a mixture of H_2O_2 and N-acetyl-L-cysteine (NAC) for 12 h prior to the addition of Lipo-FA@BODIPY11. Upon additional H_2O_2 stimulation, a more significant variation on both fluorescence channels was observed compared to the H_2O_2-free samples (Fig. 5d). Quantitative analysis revealed about a three-fold (0.91–3.01) increase of FL_{530}/FL_{610} after H_2O_2 treatment. On the other hand, the ROS scavenger, NAC, dramatically suppressed the H_2O_2 induced change on FL_{530}, FL_{610} and FL_{530}/FL_{610}. On the whole, the ratiometric fluorescence change of Lipo-FA@

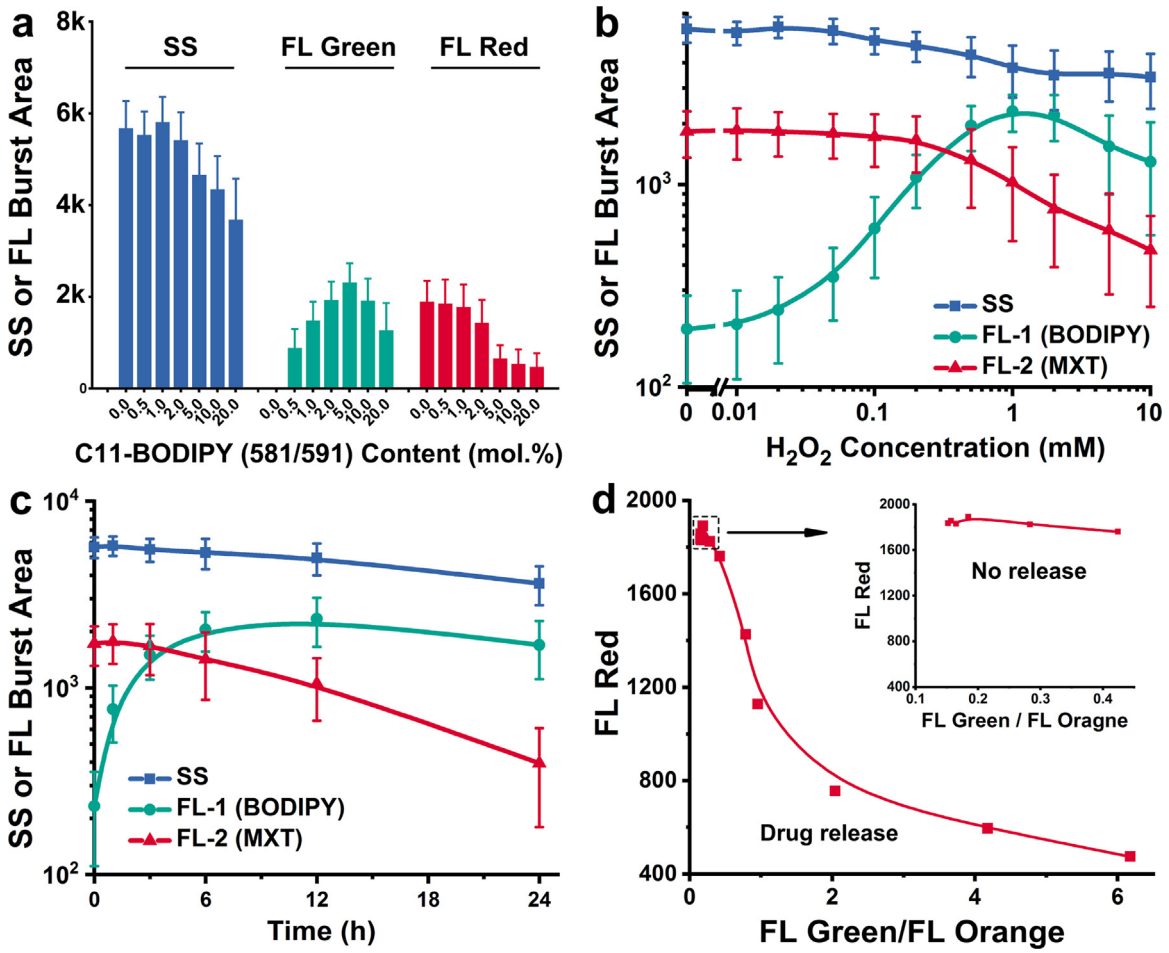

Fig. 4. Analysis of the concurrent ROS sensing and drug release behavior of Lipo@BODIPY11&MXT under various conditions. a) The H_2O_2 triggered variation on SS, green FL and red FL of Lipo@BODIPY11&MXT with different C11-BODIPY (581/591) contents. b,c) H_2O_2 concentration-dependent (b) and time-dependent (c) changes in SS, green FL and red FL intensity of Lipo@BODIPY11&MXT with 5% C11-BODIPY (581/591). d) The correlation between FL_{green}/FL_{orange} and FL_{red} derived from b). The error bars represent the interquartile range of each distribution.

BODIPY11 can be applied to detect the intracellular ROS.

As described above, the controlled MXT release was closely related to the ROS- triggered ratiometric fluorescence change. Therefore, we further investigated the intracellular drug release behavior of the folate modified, C11-BODIPY (581/591) inserted and MXT loaded liposomes (Lipo-FA@BODIPY11&MXT) by FCM. As illustrated in Fig. 6a, following folate receptor mediated endocytosis, Lipo-FA@BODIPY11&MXT was oxidized by the intracellular ROS and lead to the MXT release. Upon the interaction of MXT with mitochondria or other cellular components, more ROS were generated which triggered a ROS positive feedback loop to accelerate the MXT release (Fig. 6a). To ensure the efficient MXT release was regulated by the ROS responsive behavior of Lipo-FA@BODIPY11&MXT, liposomes without C11-BODIPY (581/591) modification (Lipo-FA@MXT) were prepared and investigated in parallel. Since the liposome encapsulated MXT exhibited very dim fluorescence due to the quenching effect, there would be a significant increase once it was released to the cytoplasm. Based on that, the fluorescence intensity on 660/20 nm (FL_{660}) of liposome treated KB cells was measured (Fig. 6b&c). It turned out that the FL_{660} intensity of Lipo-FA@BODIPY11&MXT showed a more remarkable elevation compared to Lipo-FA@MXT with the increase of incubation time. Moreover, the positive correlation between FL_{530}/FL_{610} and FL_{660} further proved that the sustained MXT release was regulated by the intracellular ROS level (Fig. 6c).

The cytotoxicity of Lipo-FA@BODIPY11 was investigated by CCK-8 assay (Fig. 6d). Empty Lipo-FA@BODIPY11 showed negligible cytotoxicity with total lipid concentration up to 100 μM. In contrast, the MXT loaded Lipo-FA@BODIPY11 displayed a concentration-dependent cytotoxicity to KB cells with IC_{50} lower than 10 μM MXT. Upon H_2O_2 treatment, the cytotoxicity of Lipo-FA@BODIPY11&MXT was notably enhanced. On the other hand, Lipo-FA@MXT without C11-BODIPY (581/591) modification displayed relatively weak cytotoxicity and showed no observable H_2O_2-dependent variation. Therefore, the enhanced cytotoxicity of Lipo-FA@BODIPY11&MXT confirmed the ROS triggered MXT release process.

4. Conclusion

Single-particle characterization of stimuli-responsive nanomaterials is fundamental to fully understand their functions and ensure reproducibility of performance. Base on the ROS-triggered ratiometric fluorescence variation and hydrophobicity change of a lipid oxidation sensor, C11-BODIPY (581/591), we fabricated a functional liposome with ROS responsive features. Taking it as a model, we developed a strategy for characterization of nanotheranostics via nFCM. By simultaneous detection of scatter light and multi-fluorescence, we were able to ensure the proper functionalization of liposomes and to assess the ROS sensing ability. Besides, we also revealed the ROS-triggered dissociation of C11-BODIPY (581/591) and the formation of aggregates for samples with high modification degree, which were otherwise masked by ensemble-averaged methods. For drug loaded samples, the reduced intensity on SS and red FL along with the increase of green FL

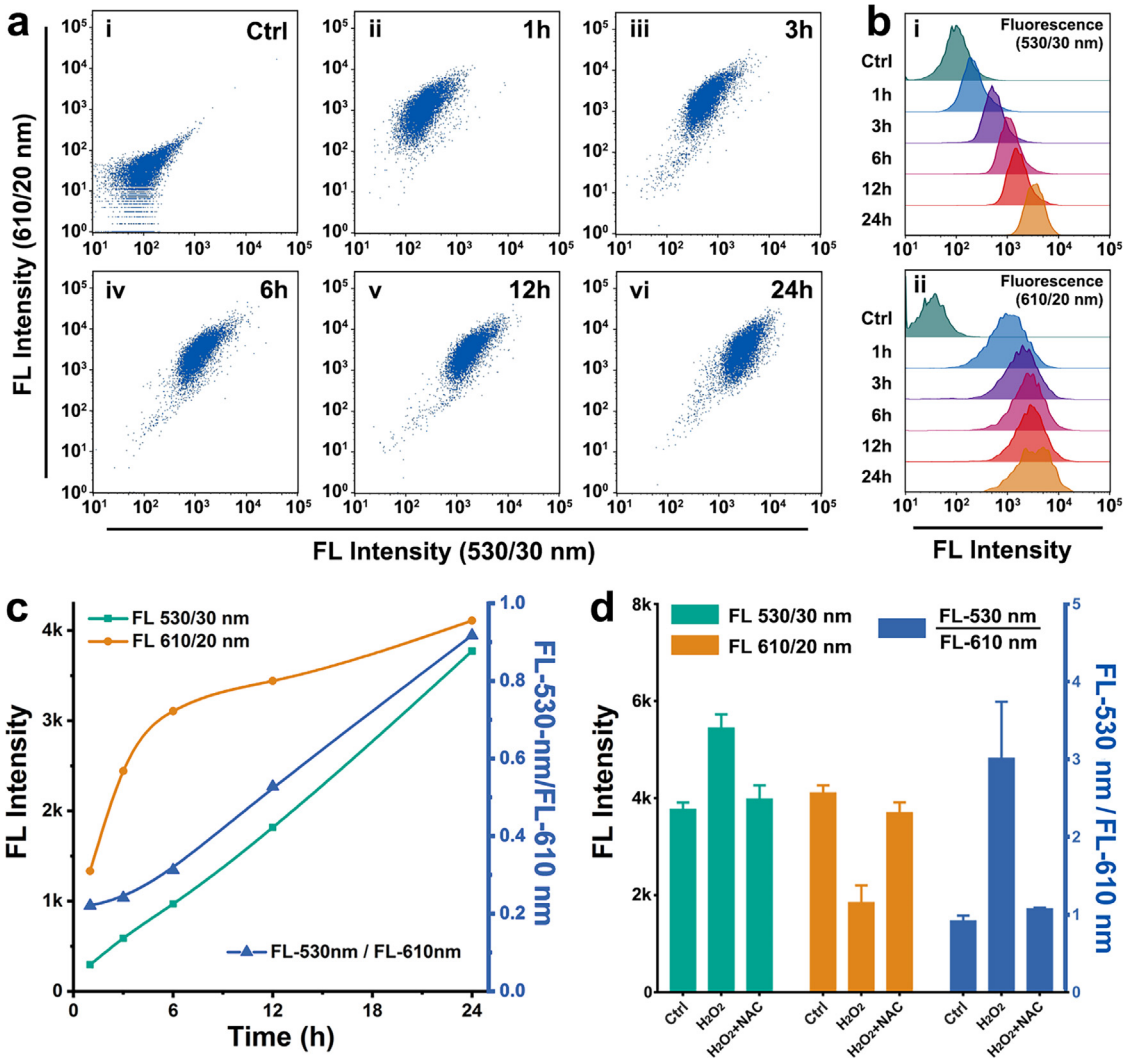

Fig. 5. FCM analysis of the intracellular ROS sensing behavior of Lipo-FA@BODIPY11 in KB cells. a) The bivariate dot-plots of green fluorescence (FL_{530}) verse orange fluorescence (FL_{610}) for KB cells incubated with Lipo-FA@BODIPY11 for different time. b) Histograms of the green and orange fluorescence intensity of KB cells incubated with Lipo-FA@BODIPY11 for different time. c) Time-dependent changes in green FL intensity, orange FL intensity and their ratio of Lipo-FA@BODIPY11 treated KB cells. d) The change in green FL intensity, orange FL intensity and their ratio of Lipo-FA@BODIPY11 treated KB cells upon various stimulations.

signal indicated a sustained drug release process, responding to the elevated H_2O_2 concentration. At last, the distinct intracellular ROS sensing and controlled drug release behavior, as well as the enhanced cytotoxicity of Lipo@BODIPY11&MXT compared with the unmodified counterpart further confirmed its applicability for theranostic purpose. This nFCM-based approach can be applied to analyze other nanotheranostics with fluorescence response modules and encapsulated with therapeutic components either exhibiting intrinsic fluorescence or can be fluorescent labeled, such as proteins and nucleic acids.

CRediT authorship contribution statement

Chaoxiang Chen: Conceptualization, Methodology, Investigation, Writing - original draft, Resources, Project administration, Funding acquisition. **Kaimin Gao:** Software, Formal analysis, Investigation, Validation. **Hong Lian:** Writing - review & editing, Visualization. **Chen Chen:** Validation, Data curation. **Xiaomei Yan:** Resources, Writing - review & editing, Supervision, Project administration, Funding acquisition.

Acknowledgements

This research was supported by the Start-up Fund of Jimei University (4411/C618004) and the National Natural Science Foundation of China (21475112 and 21627811).

Declaration of interests

The authors declare the following competing financial interest. X.Y. declare competing financial interest as a cofounder of NanoFCM Inc., a company committed to commercializing the nFCM technology.

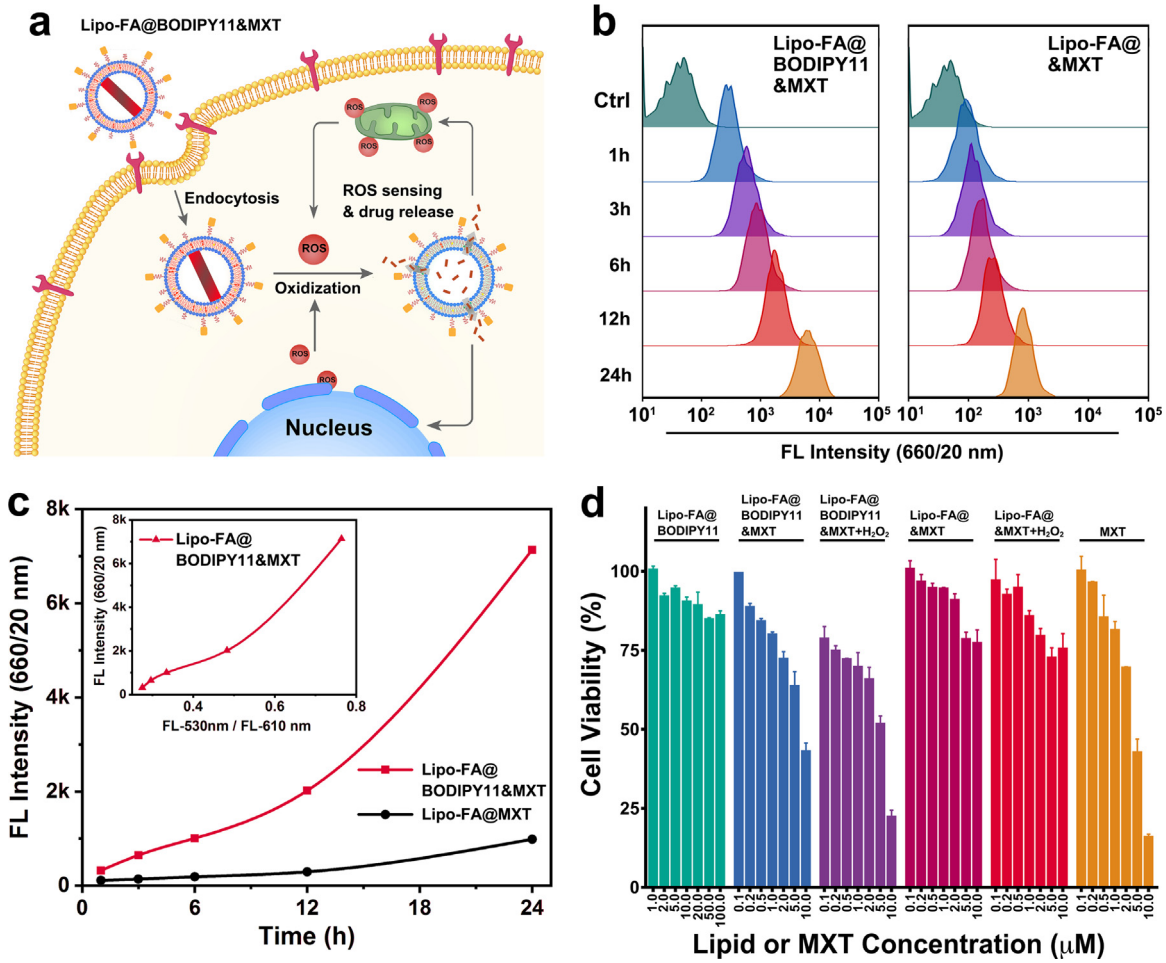

Fig. 6. Analysis of the drug release behavior and the cytotoxicity of Lipo-FA@BODIPY11&MXT. a) The schematic presentation of the endocytosis, ROS-sensing and controlled drug release behavior of Lipo-FA@BODIPY11&MXT in KB cells. b) Histograms of red fluorescence intensity distribution of KB cells incubated with Lipo-FA@BODIPY11&MXT for different time. c) Time-dependent changes in red FL intensity for KB cells incubated Lipo-FA@BODIPY11 with or without MXT encapsulation. d) Cell viability of KB cells upon various stimulation measured by the CCK-8 assay. Note: the concentration is referred to the lipid concentration for the first group and MXT concentration for the rest.

Appendix A. Supporting information

Supplementary data associated with this article can be found in the online version at doi:10.1016/j.bios.2019.02.016.

References

Bayford, R., Rademacher, T., Roitt, I., Wang, S.X., 2017. Physiol. Meas. 38, R183–R203.
Bolla, P.K., Rodriguez, V.A., Kalhapure, R.S., Kolli, C.S., Andrews, S., Renukuntla, J., 2018. J. Drug. Deliv. Sci. Technol. 46, 416–435.
Chen, C.X., Zhu, S.B., Wang, S., Zhang, W.Q., Cheng, Y., Yan, X.M., 2017a. ACS Appl. Mater. Interfaces 9, 13913–13919.
Chen, H., Zhang, W., Zhu, G., Xie, J., Chen, X., 2017b. Nat. Rev. Mater. 2, 17024.
Chen, Q., Ke, H., Dai, Z., Liu, Z., 2015. Biomaterials 73, 214–230.
Chen, Q., Liang, C., Sun, X., Chen, J., Yang, Z., Zhao, H., Feng, L., Liu, Z., 2017c. Proc. Natl. Acad. Sci. USA 114, 5343–5348.
Cho, E.J., Holback, H., Liu, K.C., Abouelmagd, S.A., Park, J., Yeo, Y., 2013. Mol. Pharm. 10, 2093–2110.
Drummen, G.P.C., Gadella, B.M., Post, J.A., Brouwers, J.F., 2004. Free Radic. Biol. Med. 36, 1635–1644.
Drummen, G.P.C., van Liebergen, L.C.M., Op den Kamp, J.A.F., Post, J.A., 2002. Free Radic. Biol. Med. 33, 473–490.
Jo, S.D., Ku, S.H., Won, Y.Y., Kim, S.H., Kwon, I.C., 2016. Theranostics 6, 1362–1377.
Karimi, M., Ghasemi, A., Sahandi Zangabad, P., Rahighi, R., Moosavi Basri, S.M., Mirshekari, H., Amiri, M., Shafaei Pishabad, Z., Aslani, A., Bozorgomid, M., Ghosh, D., Beyzavi, A., Vaseghi, A., Aref, A.R., Haghani, L., Bahrami, S., Hamblin, M.R., 2016. Chem. Soc. Rev. 45, 1457–1501.
Kim, K.S., Lee, D., Song, C.G., Kang, P.M., 2015. Nanomedicine 10, 2709–2723.
Li, C.X., Zhang, Y.F., Li, Z.M., Mei, E.C., Lin, J., Li, F., Chen, C.G., Qing, X.L., Hou, L.Y., Xiong, L.L., Hao, H., Yang, Y., Huang, P., 2018. Adv. Mater. 30, 1870049.
Li, M., Li, S., Chen, H., Hu, R., Liu, L., Lv, F., Wang, S., 2016. ACS Appl. Mater. Interfaces 8, 42–46.
Li, Y., Lin, T.Y., Luo, Y., Liu, Q., Xiao, W., Guo, W., Lac, D., Zhang, H., Feng, C., Wachsmann-Hogiu, S., Walton, J.H., Cherry, S.R., Rowland, D.J., Kukis, D., Pan, C., Lam, K.S., 2014. Nat. Commun. 5, 4712.
Liu, Y., Zhen, W., Jin, L., Zhang, S., Sun, G., Zhang, T., Xu, X., Song, S., Wang, Y., Liu, J., Zhang, H., 2018. ACS Nano 12, 4886–4893.
Mourdikoudis, S., Pallares, R.M., Thanh, N.T.K., 2018. Nanoscale 10, 12871–12934.
Muhlebach, S., Borchard, G., Yildiz, S., 2015. Nanomedicine 10, 659–674.
Mura, S., Nicolas, J., Couvreur, P., 2013. Nat. Mater. 12, 991–1003.
Muthu, M.S., Leong, D.T., Mei, L., Feng, S.S., 2014a. Theranostics 4, 660–677.
Muthu, M.S., Mei, L., Feng, S.S., 2014b. Nanomedicine 9, 1277–1280.
Patil, Y., Amitay, Y., Ohana, P., Shmeeda, H., Gabizon, A., 2016. J. Control. Release 225, 87–95.
Qian, X.Q., Han, X.X., Chen, Y., 2017. Biomaterials 142, 13–30.
Rosenblum, D., Joshi, N., Tao, W., Karp, J.M., Peer, D., 2018. Nat. Commun. 9, 1410.
Saravanakumar, G., Kim, J., Kim, W.J., 2017. Adv. Sci. 4, 1600124.
Schumacker, P.T., 2015. Cancer Cell 27, 156–157.
Tian, Y., Ma, L., Gong, M., Su, G., Zhu, S., Zhang, W., Wang, S., Li, Z., Chen, C., Li, L., Wu, L., Yan, X., 2018. ACS Nano 12, 671–680.
Wang, J., Tao, W., Chen, X., Farokhzad, O.C., Liu, G., 2017. Theranostics 7, 3915–3919.
Yang, Z., Dai, Y., Yin, C., Fan, Q., Zhang, W., Song, J., Yu, G., Tang, W., Fan, W., Yung, B.C., Li, J., Li, X., Li, X., Tang, Y., Huang, W., Song, J., Chen, X., 2018. Adv. Mater. 30, e1707509.
Zhang, H., 2017. Methods Mol. Biol. 1522, 17–22.
Zhang, M., Song, C.C., Su, S., Du, F.S., Li, Z.C., 2018. ACS Appl. Mater. Interfaces 10, 7798–7810.
Zhu, S., Ma, L., Wang, S., Chen, C., Zhang, W., Yang, L., Hang, W., Nolan, J.P., Wu, L., Yan, X., 2014. ACS Nano 8, 10998–11006.
Zwicke, G.L., Mansoori, G.A., Jeffery, C.J., 2012. Nano Rev. 3, 18496.